Numerical Solution of Natural Convection in Eccentric Annuli

Darrell W. Pepper* and Roger E. Cooper†
E. I. du Pont de Nemours & Co., Aiken, South Carolina

The governing equations for transient natural convection in eccentric annular space are solved with two high-order accurate numerical algorithms. The equation set is transformed into bipolar coordinates and split into two one-dimensional equations: finite elements are used in the direction normal to the cylinder surfaces; the pseudospectral technique is used in the azimuthal direction. Transient solutions of the entire flowfield are obtained for $10^2 \le Ra \le 10^6$, $0.70 \le Pr \le 10^2$, with the inner cylinder near the top, bottom, and side of the outer cylinder. Results are similar to experimental and numerical values previously published for low *Ra* numbers.

Nomenclature

A = $c/(\sin\S \sinh\eta)$
B = $(1-\cosh\eta\cos\S)/(\sin\S\sinh\eta)$
c = $r_i \sinh\eta_i = r_o \sinh\eta_o$
D = $(\cosh\eta-\cos\S)^2/(c\sin\S\sinh\eta)$
e = eccentricity, $x_o - x_i$
g = acceleration of gravity
h_i = heat transfer coefficient
J = Jacobian
k = PrD or D
k = wavenumber
K_{eq} = local equivalent conductivity
L = cavity gap
N_u = Nusselt number
Pr = Prandtl number, ν/α'
Q = temperature gradient components of vorticity equation
q = heat flux, $2\pi h_i (T_i' - T_o')$
r = radial direction
Ra = Rayleigh number, $g\beta(T_i'-T_o')L^3/\nu\alpha'$
r_i = radius of inner cylinder
r_o = radius of outer cylinder
t = $\alpha' t'/L^2$
t' = time
T = $(T'-T_o')/(T_o-T_i')$
T' = internal temperature
T_i' = temperature of inner cylinder wall
T_o' = temperature of outer cylinder wall
u = $u'L/\alpha'$
u' = velocity component in the x direction
v = $v'L/\alpha'$
v' = velocity component in the y direction
w = $L^2 w'/\nu$
w' = vorticity
x = x'/L
x' = vertical direction, rectangular coordinate
y = y'/L
y' = horizontal direction, rectangular coordinate
α = angle of rotation of x,y axis
α' = thermal diffusivity
β = thermal expansion coefficient
γ = r_i/r_o
Δ = grid interval
$\S$ = bipolar coordinate, normal to η
η = bipolar coordinate, normal to $\S$
θ = azimuthal direction ($\approx \S$)
λ = $e/(r_o - r_i)$
ν = kinematic viscosity
Ψ = $\Psi'/L\alpha'$
Ψ' = streamfunction
ϕ = time-dependent variable
∇^2 = $\partial^2/\partial^2 + \partial^2/\partial y^2$
$\bar{\nabla}^2$ = $\partial^2/\partial\S^2 + \partial^2/\partial\eta^2$

Subscripts

cd = conduction
cv = convection
i = inner cylinder wall
o = outer cylinder wall
α = rotated x, y axis

Presented as Paper 82-0983 at the AIAA/ASME Third Joint Thermophysics, Fluids, Plasma and Heat Transfer Conference, St. Louis, Mo., June 7-11, 1982; submitted June 11, 1982; revision submitted Dec. 27, 1982.

*Research Supervisor, Nuclear Engineering Division, Savannah River Laboratory.

†Research Engineer, Environmental Transport Division, Savannah River Laboratory.

Introduction

NATURAL convection in concentric annuli has been studied for many years. Numerous articles can be found in the literature which describe both experimental and numerical results.[1-4] Natural convection in eccentric annular space, although not analyzed as extensively, has begun to receive more attention over the last few years. Natural convection heat transfer in eccentric annuli occurs in many industrial situations. Such problems commonly occur within the electric and nuclear energy fields, as well as in the solar energy and thermal storage systems. For example, the cooling of underground electric transmission cables is affected significantly by the position of the inner cable within the outer housing. Similarly, the cooling of nuclear fuel and target tube assemblies following irradiation must be monitored carefully in the event of assembly burnout due to inner tubular eccentricities. Likewise, natural convection cooling of casks containing nuclear waste can exceed thermal guidelines if positioning becomes overly eccentric. In this study free convection flow within an eccentric annulus is solved numerically using bipolar coordinate transformation and one-dimensional finite element and pseudospectral algorithms. Steady-state results are compared with existing theoretical and experimental data.

Forced convection in eccentric annuli was investigated by Trombetta[5] using approximation methods and a least-squares technique for various radius ratios and eccentricity. Similar studies for laminar flow through an eccentric annulus was made by Guckes.[6] Both Newtonian and non-Newtonian fluid flows were calculated using bipolar coordinates and a finite difference technique. An analytical study of free convection in eccentric annuli was conducted by Yao,[7] using perturbation techniques with the eccentric space transformed into a unit

circle. Analytical solutions were obtained for slightly eccentric annuli with $Ra \leq 10^4$ for constant cylinder wall temperatures.

Both numerical and experimental studies of natural convection and thermal conduction in annular regions were undertaken by Ratzel et al.[8] A finite element procedure using isoparametric elements was employed. Cylinder walls were held constant; the inner cylinder temperature was allowed to vary. Steady-state streamline and isotherm distributions in concentric regions were obtained for $3\times10^2 \leq Ra \leq 9.7\times10^4$; eccentric annular distributions were obtained for $1.2\times10^4 \leq Ra \leq 2.2\times10^4$.

Free convection flow in eccentric annuli was modeled by Projahn et al.[9] using body-fitted curvilinear coordinate transformations[10] and the strongly implicit finite difference procedure. Solutions were obtained in the half-plane for varying vertical eccentricities. Results for both horizontal and vertical eccentricities were compared with data obtained by Kuehn and Goldstein.[11] Bipolar coordinate transformations have also been used recently to calculate flow and temperature distributions through an eccentric annular duct by Feldman et al.,[12,13] following the work of Synder and Goldstein.[14]

Recently, Prusa and Yau[15] numerically simulated eccentric annular free convection between two cylinders for Grashof numbers $\leq$16,900 and various vertical displacements of the inner cylinder. The governing equations for steady laminar flow in polar coordinates were nondimensionalized and transformed into a unit circle (the boundary of the inner cylinder becomes a pole at the center of the unit circle). The transformed equations were solved for one half of the circular domain using finite differences with several mesh spacings. Computation times ranged from 50 s to several hours on a CDC 175 for 10^{-4} residual convergence. Results agreed favorably with experimental data and analytical solutions obtained using perturbation techniques at low Grashof numbers.[7]

Problem Analysis

The problem to be analyzed consists of free convective flow developed in the cross section of an eccentric annulus, as shown in Fig. 1. The geometry and configuration lends itself readily to bipolar coordinates; e.g., Synder,[16] El-Saden,[17] and Redberger and Charles.[18] Transformation from rectangular (x,y) to bipolar coordinates $(\S,\eta)$ is obtained from the relations

$$x = \frac{c\sinh\eta}{\cosh\eta - \cos\S} \tag{1a}$$

$$y = \frac{c\sin\S}{\cosh\eta - \cos\S} \tag{1b}$$

where $c = r_i\sinh\eta_i = r_o\sinh\eta_o$ and η_i and η_0 denote inner and outer annulus surfaces defined as

$$\eta_i = \cosh^{-1}\left[\frac{\gamma(1+\lambda^2)+(1-\lambda^2)}{2\lambda\gamma}\right] \tag{2a}$$

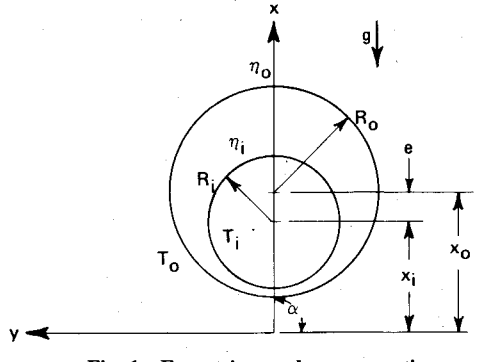

Fig. 1 Eccentric annular cross section.

$$\eta_o = \cosh^{-1}\left[\frac{\gamma(1-\lambda^2)+(1+\lambda^2)}{2\lambda}\right] \tag{2b}$$

with $\gamma = r_i/r_o$ and $\lambda = e/(r_o - r_i)$.

The inner surface, as depicted in Fig. 1, is assumed to be heated to constant temperature T_i. The outer surface is held constant at a lower temperature T_o, thus establishing a temperature differential which leads to free convective flow.

The governing equations are defined in bipolar coordinates as (see Appendix):

$$A\frac{\partial w}{\partial t} - \frac{\partial uw}{\partial\S} + B\frac{\partial uw}{\partial\eta} - B\frac{\partial vw}{\partial\S} - \frac{\partial vw}{\partial\eta}$$

$$= PrD\bar{\nabla}^2 w + PrRa\left(B\frac{\partial T}{\partial\S} + \frac{\partial T}{\partial\eta}\right) \tag{3}$$

$$A\frac{\partial T}{\partial t} - \frac{\partial uT}{\partial\S} + B\frac{\partial uT}{\partial\eta} - B\frac{\partial vT}{\partial\S} - \frac{\partial vT}{\partial\eta} = D\bar{\nabla}^2 T \tag{4}$$

$$\bar{\nabla}^2\Psi = -(A/D)\,w \tag{5}$$

The velocities, u and v, are defined as

$$u = -\frac{1}{c}\left[(1-\cosh\eta\cos\S)\frac{\partial\Psi}{\partial\S} + \sinh\eta\sin\S\frac{\partial\Psi}{\partial\eta}\right] \tag{6}$$

$$v = \frac{1}{c}\left[\sinh\eta\sin\S\frac{\partial\Psi}{\partial\S} - (1-\cosh\eta\cos\S)\frac{\partial\Psi}{\partial\eta}\right] \tag{7}$$

The boundary conditions associated with Eqs. (3-5) are

$$T(\eta_i,\S) = 1,\quad T(\eta_o,\S) = 0,\quad T(\eta,-\pi) = T(\eta,\pi) \tag{8}$$

$$\Psi(\eta_i,\S) = \Psi(\eta_o,\S) = 0,\quad \Psi(\eta,-\pi) = \psi(\eta,\pi) \tag{9}$$

$$w(\eta_i,\S) = w(\eta_o,\S) = -\frac{D}{A}\frac{\partial^2\Psi}{\partial\eta^2},\quad w(\eta,-\pi) = w(\eta,\pi) \tag{10}$$

Numerical Solution Technique

Application of bipolar coordinates results in the physical plane being transformed into a rectangular domain,[18,19] as shown in Fig. 2. A finite element recursion relation[20] and a pseudospectral method[21,22] are used to solve Eqs. (3) and (4). Equation (5) is solved by cyclic reduction.[23]

The problem is strongly governed by the nonperiodic η boundary conditions, for which the finite element technique is well suited. The pseudospectral method is ideal for periodic boundary-value problems, as established by the conditions at $\S = -\pi,\ \pi$. Cubic spline techniques and other compact operators are also viable alternatives to solving the equation set.

Equations (3) and (4) are solved in a fractional sequence, allowing the equation set to be solved with basic one-dimensional algorithms. The resulting equation system is

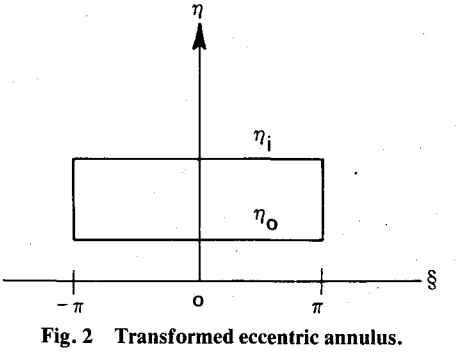

Fig. 2 Transformed eccentric annulus.

solved sequentially in each coordinate direction. The advantages of using these methods over more conventional finite difference methods lie in their high-order accuracy, equivalent computational speed, and ease of implementation.

Application of the techniques is straightforward. For example, Eq. (3) is first split into two equations

$$A\frac{\partial w^*}{\partial t} - \frac{\partial uw}{\partial \S} - B\frac{\partial vw}{\partial \S} = PrD\frac{\partial^2 w}{\partial \S^2} + PrRaB\frac{\partial T}{\partial \S} \tag{11a}$$

$$A\frac{\partial w}{\partial t} + B\frac{\partial uw^*}{\partial \eta} - \frac{\partial vw^*}{\partial \eta} = PrD\frac{\partial^2 w^*}{\partial \eta^2} + PrRa\frac{\partial T}{\partial \eta} \tag{11b}$$

where w^* denotes intermediate vorticity values. A similar sequence is performed for Eq. (4). For a one-dimensional uniform element length, the basic recursion relation for the η direction Eq. (11b) is written as[20]

$$\frac{1}{6}[\dot\phi_{i-1} + 4\dot\phi_i + \dot\phi_{i+1}] + \frac{1}{6\Delta\eta}[\phi_{i-1}(-u_{i-1} - 2u_i) + \phi_i(u_{i-1} - u_{i+1}) + \phi_{i+1}(2u_i + u_{i+1})] + \frac{k}{\Delta\eta^2}(-\phi_{i-1} + 2\phi_i - \phi_{i+1}) = Q \tag{12}$$

where u_i is the velocity at node point i, ϕ is either vorticity or temperature, $\dot\phi$ denotes the time derivative, k is either PrD or D according to the equation being solved, and Q is the temperature gradient term (or zero).

A simple tridiagonal algorithm is used to solve the equation. The time-derivative terms are expressed as new and old values using Crank-Nicolson time averaging. Boundary relations at η_i and η_o are expressed by assembling the element expression over one element, i.e., the boundary and first interior node.[20]

Upon solution of the one-dimensional transport equation in the η direction, ϕ is solved in the § direction by a one-dimensional pseudospectral technique. The time-dependent Fourier components $A(k,t)$ in one-dimensional spectral space are determined from the distribution of ϕ in physical space, i.e.,

$$A(k,t) = \frac{1}{N}\sum_{\S}\phi\exp(ik\S) \tag{13}$$

where N is the number of mesh points spanning the § coordinate direction, i is $\sqrt{-1}$, t time, and k the wavenumber defined as

$$k \equiv k_j = 2\pi n_j/\Delta\S N, \qquad j = 1,\ldots N \tag{14}$$

where n_j assumes integer values as $-N/2 < n_j < N/2$. After the Fourier components are obtained, the derivatives are evaluated directly by the relations

$$\frac{\partial\phi}{\partial\S} = \sum_k ik_j A(k,t)\exp(ik\S) \tag{15a}$$

$$\frac{\partial^2\phi}{\partial\S^2} = \sum_k -k_j^2 A(k,t)\exp(ik\S) \tag{15b}$$

These transforms are evaluated using a fast Fourier transform algorithm.[24] Periodicity of the boundary conditions, as imposed by Eq. (10), is accommodated easily by the pseudospectral technique. Equation (11a) is solved using the values obtained for the spatial derivatives and forward-in-time differencing.

Results

Solutions to the transformed equation set were calculated for $10^2 \le Ra \le 10^6$. Solutions were begun with w and T set to zero within the computational domain for $Ra \le 10$. A 20×20 mesh was used with $\Delta\S = 0.331$, $\Delta\eta = 0.040$, and $\Delta t = 0.001$. Computations were made on an IBM 3081; an average of 500 iterations were required to achieve 10^{-3} convergence for vorticity $[(W_{new} - W_{old})/W_{old}]$. Studies were conducted with the inner cylinder oriented near the bottom, top, and side of the outer cylinder.

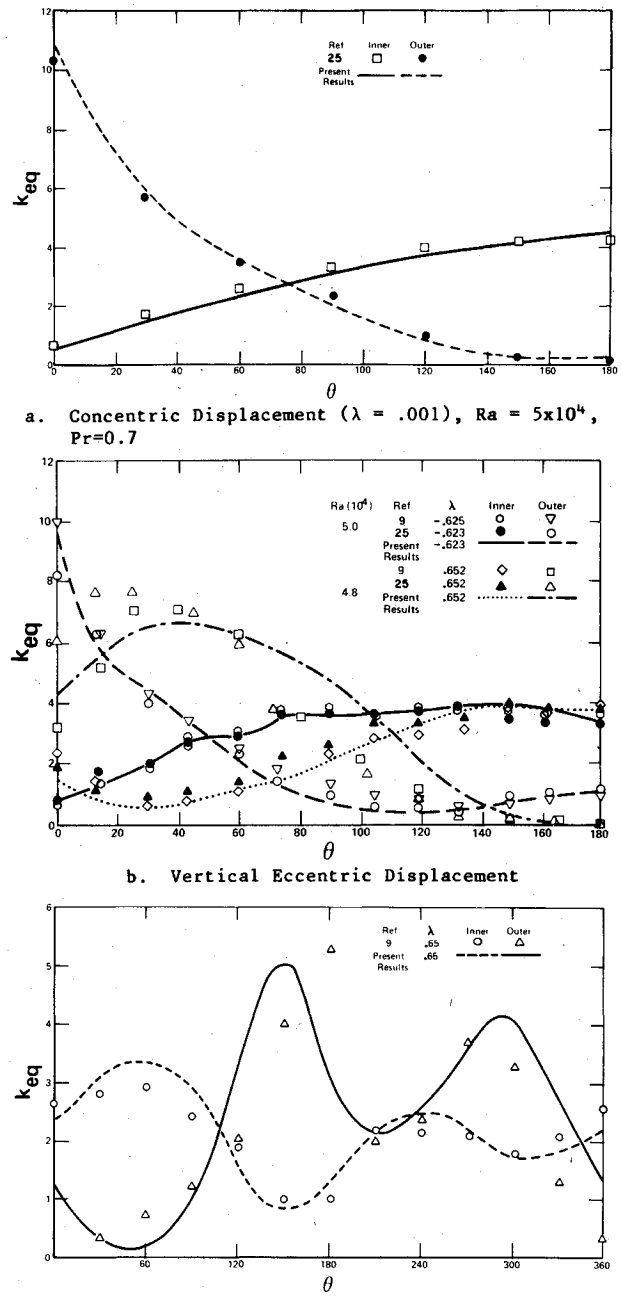

Fig. 3 Local equivalent conductivity vs angular position.

To assess model accuracy, a nearly concentric ($\lambda = 0.001$) case was simulated, and values of local equivalent conductivity,[25,26] K_{eq}, vs azimuthal location ($\S = \theta$) compared with values obtained by Projahn et al.[9] and Kuehn and Goldstein[25] for $Ra = 5 \times 10^4$, $Pr = 0.7$, and $\gamma = 2.6$. A perfectly concentric situation is not possible using bipolar coordinates as $\lambda = 0$ causes the equations to become degenerate. Figure 3a compares results from the present study with both experimental and numerical data.[9,23] The model predicts similar conductivity values for the concentric case. Figure 3b shows comparisons for two eccentric cases, $\lambda = 0.652$ and $\lambda = -0.623$. Ra values for $\lambda = 0.652$ (near the top of the outer cylinder) and $\lambda = -0.623$ (bottom) were 4.8×10^4 and 5×10^4,

respectively. The appearance of a premature maximum in the outer cylinder for K_{eq} and $\lambda = 0.652$ at $\theta \cong 40$ deg was also observed by Prusa and Yao[15] for Grashof number equal to 16,900. This effect is due to flow inhibition between the two cylinder surfaces; convection heat transfer decreases and conduction increases as $\theta \to 0$ deg. Model predictions for K_{eq} vs θ agree fairly well in the remaining configurations with published data.[9,15,25] Figure 3c shows equivalent conductivity values with the inner cylinder offset laterally from the center of the outer cylinder for $\lambda = 0.65$ and $Ra = 10^4$. Results from the present model are not in close agreement with results obtained by Projahn et al.,[9] but appear to follow the same general trend and curve shape.

Streamline and isotherm plots are shown in Figs. 4 and 5 for $Ra = 10^2$-10^6 with $\lambda = -0.625$ and $\lambda = 0.625$, respectively. The flowfield and temperature distributions are essentially symmetric. Half-plane results obtained by Projahn et al.[9] are similar in appearance; differences in values are principally due to boundary conditions and coordinate transformations employed, mesh size, and the order of numerical accuracy between finite difference and Galerkin methods. An increase in Rayleigh number creates an increase in overall strength and circulation pattern for all orientations of the inner cylinder. Positioning the inner cylinder toward the bottom of the outer cylinder increases the overall heat transfer and flow strength, and supports similar conclusions obtained in previous studies.[9,15,25] Solutions tended to be independent of Prandtl number when $Pr > 10$.

Velocity vector plots are shown in Figs. 6a-c for $Ra = 10^4$ and $Ra = 10^5$ with $\lambda = \pm 0.325$ and $\lambda = \pm 0.625$. Vectors without tails denote very low velocities. Two large recirculating cells appear within the annular space between the two cylinders, as previously shown in Figs. 4 and 5. As the fluid approaches the cylinder walls, velocity gradients become large and the local heat transfer increases. The effect of increasing the eccentricity is shown by comparing Figs. 6a and 6b for $Ra = 10^4$. An increase in velocity (and cell strength) occurs as λ increases from -0.325 to -0.625. As the flow approaches the top of the inner cylinder, buoyancy causes the fluid to become more vertically oriented. The boundary layer decelerates at the top of the inner cylinder and separates from the surface; the flow becomes entrained within the thermal plume. Upon hitting the outer cylinder wall, the flow cools very rapidly and travels downward. Conduction heat transfer dominates between the two cylinders at the bottom of the inner cylinder; convection becomes dominant as the flow

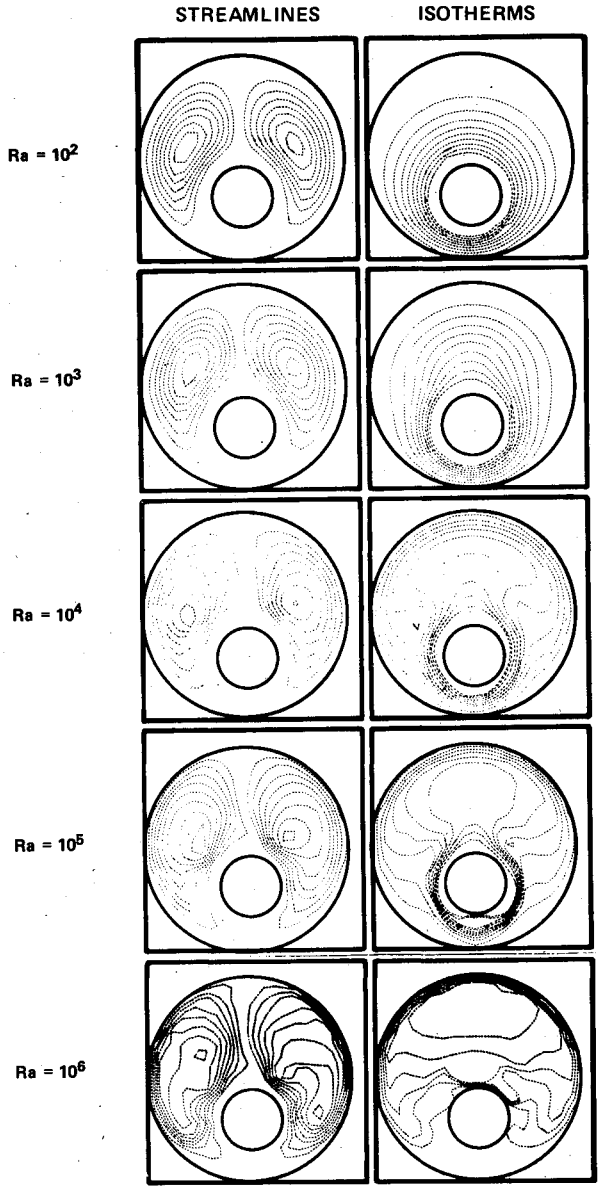

Fig. 4 Streamlines and isotherms for $Ra = 10^2$-10^6, $r_o/r_i = 2.6$, $\lambda = -0.625$.

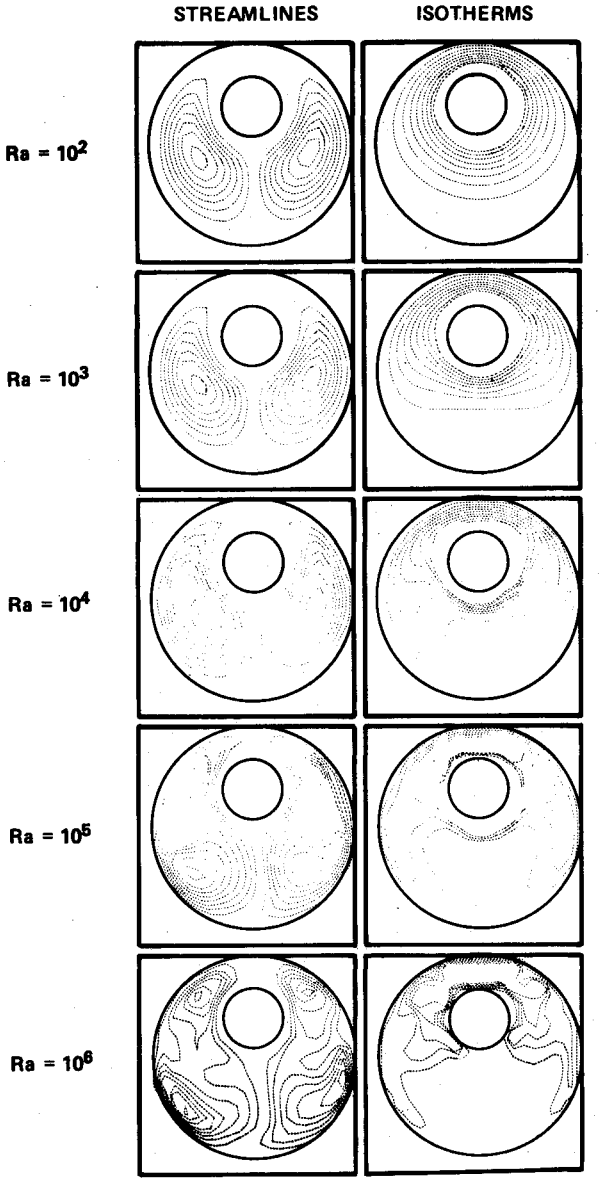

Fig. 5 Streamlines and isotherms for $Ra = 10^2$-10^6, $r_o/r_i = 2.6$, $\lambda = 0.625$.

travels around the inner surface. In this configuration the annular space is sufficiently large enough to permit smooth deceleration of velocity; this leads to the development of a strong vortex as the flow returns to the heated inner cylinder.

Velocity vectors for the positive eccentric case also show large velocity gradients near the inner and outer cylinder walls. Conduction now becomes the dominant mechanism of heat transfer in the annular space at the top of the inner cylinder. As the fluid returns along the outer cylinder wall, the flow cools and approaches a region of relatively stagnant fluid where convection is weak. This region is also evident in Fig. 5. The effect of convection becomes more inhibited in the region between the inner and outer cylinders for $\lambda = 0.625$; this is understandable since the upper region is now inadequate to permit rapid acceleration of fluid motion around the inner cylinder.

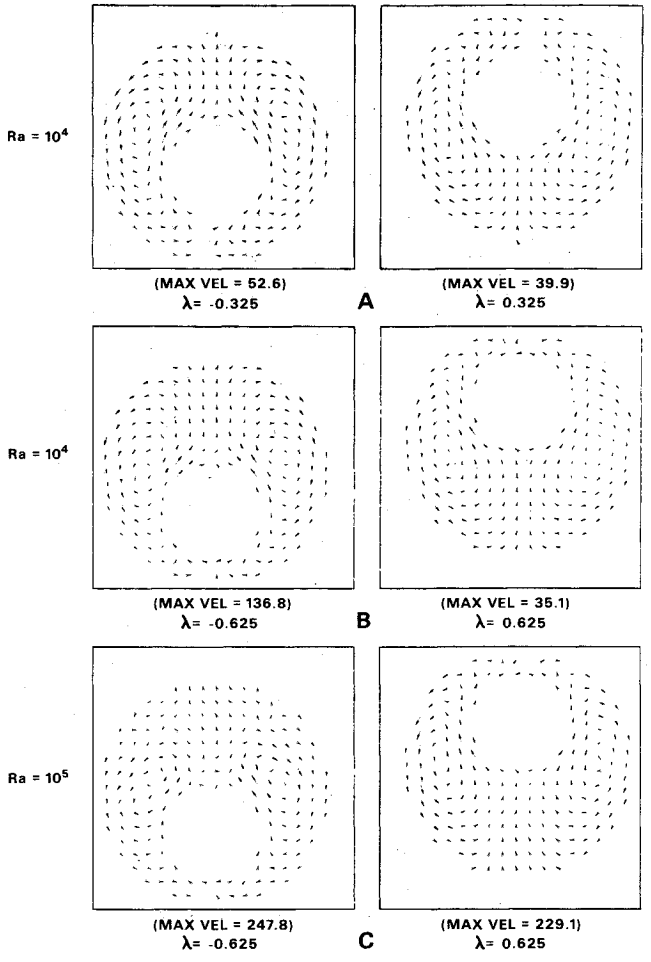

Fig. 6 Velocity vectors for $Ra = 10^4$-10^5 with $\lambda = \pm 0.325$ and $\lambda = \pm 0.625$.

The effect of increasing the Rayleigh number is shown in Figs. 6b and 6c. In this instance, $\lambda = \pm 0.625$, while the Rayleigh number is increased from 10^4 to 10^5. As expected, the velocities increase significantly for both displacements, and the velocity gradients become steeper near the cylinder walls. The onset of a small secondary vortex is just beginning to appear for $\lambda = -0.625$ immediately above the two large cells adjacent to the inner cylinder. For $\lambda = 0.625$, the increase in Rayleigh number increases the flow velocity and cell strength; however, the two large cells shift slightly upward and the bottom stagnant region appears relatively unchanged.

It is apparent that the mesh spacing near the cylinder walls cannot resolve accurately the boundary-layer development and local flow behavior for problems where $Ra \geq 10^5$. Although the mesh is somewhat coarse, the numerical methods do provide a reasonable approximation to the bulk fluid motion and temperature pattern.

A plot of the overall Nusselt number $\bar{Nu}$ vs Rayleigh number is shown in Fig. 7 for $\gamma = 2.6$ and $\lambda = 0.325$ with $Pr = 0.7$ and 100. The average Nusselt number is based on the local values at $r = r_i$ and $r = r_o$ (Ref. 25). Results are in close agreement with values obtained by Kuehn and Goldstein.[11] The transformed relation for the inner Nusselt number (convection) is

$$Nu_i = -\frac{(r_o - r_i)}{2\pi\Delta T}\int_{-\pi}^{\pi}\left(\frac{\cos\S - \cosh\eta_i}{c}\right)\frac{\partial T}{\partial \eta}\,d\S \tag{16}$$

which is integrated to yield an overall Nusselt number at r_i. The integral in Eq. (16) is solved by Simpson's rule. A similar relation is obtained for the value at $r = r_o$. The mode of heat transfer is essentially one of conduction at low Ra numbers ($\leq 10^3$). The Nusselt number for conduction is obtained using the equation[8,25]

$$Nu_{cd} = \frac{2}{\cosh^{-1}[(r_o^2 + r_i^2 - e^2)/2r_o r_i]} \tag{17}$$

The overall Nusselt number is calculated by the relation

$$Nu = [Nu_{cv}^{15} + Nu_{cd}^{15}]^{1/15} \tag{18}$$

where Nu_{cv} is the averaged overall Nusselt number for convection.

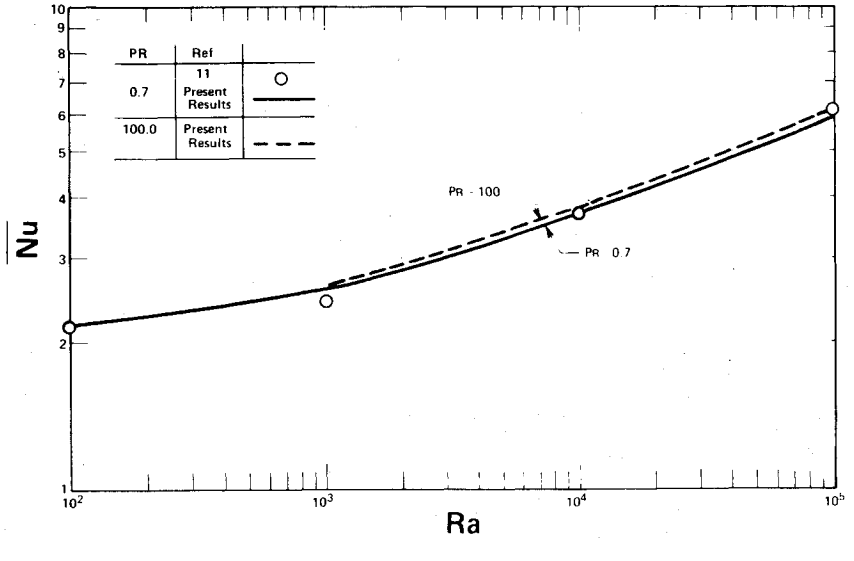

Fig. 7 Overall Nusselt number vs Rayleigh number for $\lambda = -0.325$.

Equation (18) is used to compromise the effects of both conduction and convection in obtaining the overall Nusselt number. The exponential value of 15 was chosen by Kuehn and Goldstein[25] to fit experimental data, and was used similarly in this study to compare with their results.

The effect of position of the inner cylinder significantly influences the local Nusselt numbers. A decrease in the inner Nusselt number occurs when the inner cylinder is moved toward the upper region of the outer cylinder; accordingly, the outer Nusselt number increases. An increase in Prandtl number (≤ 100) creates only a slight increase in the overall Nusselt number.

Conclusions

The solution of natural convection flow in the eccentric annular space between two isothermal cylinders has been obtained for $10^2 \leq Ra \leq 10^6$ and $0.7 \leq Pr \leq 10^2$. The transient equation set of vorticity and temperature was transformed from rectangular to bipolar coordinates and solved with two high-order accurate one-dimensional algorithms. A linear finite element recursion relation was used to solve the transport equations normal to the cylinder surfaces; a pseudospectral technique was used to solve the periodic equations tangential to the surfaces. Both algorithms are simple to use and computationally efficient.

Computational damping and dispersion errors associated with both methods are low, (especially in the pseudospectral method). The abilities of both methods to resolve steep gradients is well documented in the literature. The use of one-dimensional algorithms keeps core requirements and computational time small; less than 100-k byte storage was required for the problems addressed in this study. Steady-state solutions were achieved within approximately 1.5 min CPU for $Ra \geq 10^5$ on an IBM 3081 computer.

Computational results support data previously published in the literature. In negative eccentric displacements heat transfer rates are greater than in concentric configurations. Heat transfer rates are lowest when the inner cylinder is displaced upward toward the outer cylinder. In horizontally eccentric configurations, local conductivities are nearly symmetric about each vertical half-plane; streamlines and isotherms are displaced slightly from the midplane axis.

As the Prandtl number increases, heat transfer rates increase slightly; the recirculation center tends to shift slightly upward for $Pr > 10$ in concentric and negative displacement positions. A multicellular flow regime begins to develop for vertical eccentricities when $Ra \approx 10^5$; flows appear to be nearly symmetric within the entire plane. At $Ra = 10^6$, a multicellular flow regime is developed but no flow oscillations occur, although the flows slightly asymmetric.

Appendix

The governing equations for free convection flow can be written in rectangular coordinates and nondimensional variables[20] as

$$\frac{\partial w}{\partial t} + u\frac{\partial w}{\partial x} + v\frac{\partial w}{\partial y} = Pr\nabla^2 w - PrRa\frac{\partial T}{\partial y} \tag{A1}$$

$$\frac{\partial T}{\partial t} + u\frac{\partial T}{\partial x} + v\frac{\partial T}{\partial y} = \nabla^2 T \tag{A2}$$

$$\nabla^2 \Psi = -w \tag{A3}$$

and u and v are the velocity components defined as

$$u = \frac{\partial \Psi}{\partial y} \tag{A4}$$

$$v = -\frac{\partial \Psi}{\partial x} \tag{A5}$$

Transformation of Eqs. (A1-A3) to bipolar coordinates are performed by use of the chain rule and Eqs. (1) and (2) in the text. First-derivative terms are transformed readily by employing the inverse Jacobian matrix (J^{-1}) such that

$$\begin{Bmatrix} \frac{\partial}{\partial x} \\ \frac{\partial}{\partial y} \end{Bmatrix} J^{-1} = \begin{Bmatrix} \frac{\partial}{\partial \S} \\ \frac{\partial}{\partial \eta} \end{Bmatrix} \tag{A6}$$

where J^{-1} is defined as

$$J^{-1} = \frac{1}{c}\begin{bmatrix} -\sinh\eta\sin\S & 1-\cosh\eta\cos\S \\ \cosh\eta\cos\S - 1 & -\sinh\eta\sin\S \end{bmatrix} \tag{A7}$$

Second-derivative terms come from repeated application of the chain rule and Eq. (A7). Thus, ∇^2 becomes

$$\nabla^2 = \left(\frac{\cosh\eta - \cos\S}{c}\right)^2 \bar{\nabla}^2 \tag{A8}$$

Temperature is held fixed at $r = r_i$ and $r = r_o$. Calculations involving the Nusselt number require temperature gradients normal to the two cylinder surfaces, i.e., $(\partial T/\partial r)/r_i, r_o$. The derivative $\partial T/\partial r$ is transformed by the relation

$$\frac{\partial T}{\partial r} = \frac{\partial T}{\partial x}\cos\alpha + \frac{\partial T}{\partial y}\sin\alpha \tag{A9}$$

and employment of Eq. (A6); thus, Eq. (A9) becomes

$$\frac{\partial T}{\partial r} \equiv \left(\frac{\cos\S - \cosh\eta}{c}\right)\frac{\partial T}{\partial \eta} \tag{A10}$$

A preliminary transformation of the equation can be made if the inner cylinder is horizontally displaced (rotated) in the y direction. A simple axis rotation of the rectangular coordinates can be made prior to transforming to bipolar coordinates, i.e.,

$$\begin{Bmatrix} x' \\ y' \end{Bmatrix} = \begin{bmatrix} \cos\alpha & -\sin\alpha \\ \sin\alpha & \cos\alpha \end{bmatrix}\begin{Bmatrix} x'\alpha \\ y'\alpha \end{Bmatrix} \tag{A11}$$

Acknowledgment

The information contained in this article was developed during the course of work under Contract DE-AC09-76SR00001 with the U.S. Department of Energy.

References

[1] Powe, R. E., Corley, C. T., and Carrath, S. L., "A Numerical Solution for Natural Convection in Cylindrical Annuli," *Journal of Heat Transfer*, Vol. 93, May 1971, pp. 210-220.

[2] Charrier-Mojtabi, M. C., Mojtabi, A., and Caltagirone, J. P., "Numerical Solution of a Flow Due to Natural Convection in Horizontal Cylindrical Annulus," *Journal of Heat Transfer*, Vol. 101, 1979, pp. 171-173.

[3] Custer, J. R. and Shaughnessy, E. J., "Natural Convection in Liquid Metals in an Enclosure," *Journal of Heat Transfer*, Vol. 99, 1977, pp. 675-676.

[4] Schwab, T. H. and de Witt, K. J., "Numerical Investigation of Free Convection between Two Vertical Coaxial Cylinders," *A.I.Ch.E. Journal*, Vol. 16, 1970, pp. 1005-1010.

[5] Trombetta, M. L., "Laminar Forced Convection Eccentric Annuli," *International Journal of Heat and Mass Transfer*, Vol. 14, 1971, pp. 1161-1173.

[6] Guckes, T. L., "Laminar Flow of Non-Newtonian Fluids in an Eccentric Annulus," *Journal of Engineering for Industry*, Vol. 97, ASME, May 1975, pp. 498-506.

[7] Yao, L. S., "Analysis of Heat Transfer in Slightly Eccentric Annuli," *Journal of Heat Transfer*, Vol. 102, 1980, pp. 279-284.

[8] Ratzel, A. C, Hickox, C. E., and Gartling, D. K., "Techniques for Reducing Thermal Conduction and Natural Convection Heat Losses in Annular Receiver Geometries," *Journal of Heat Transfer*, Vol. 101, 1979, pp. 108-113.

[9] Projahn, V., Reiger, H., and Beer, H., "Numerical Analysis of Laminar Natural Convection Between Concentric and Eccentric Cylinders," *Numerical Heat Transfer*, Vol. 4, 1981, pp. 131-146.

[10] Thompson, J. F., Thames, F. C., and Mastin, C. W., "Automatic Numerical Generation of Body-Fitted Curvilinear Coordinate System for Fields Containing any Number of Arbitrary Two-Dimensional Bodies," *Journal of Computational Physics*, Vol. 15, 1974, pp. 229-310.

[11] Kuehn, N. H. and Goldstein, R. J., "Correlating Equations for Natural Convection Heat Transfer Between Horizontal Circular Cylinders," *International Journal of Heat and Mass Transfer*, Vol. 10, 1976, pp. 1127-1134.

[12] Feldman, E. E., Hornbeck, R. W., and Osterle, J. F., "A Numerical Solution of Laminar Developing Flow in Eccentric Annular Ducts," *International Journal of Heat and Mass Transfer*, Vol. 25, No. 2, 1982, pp. 231-241.

[13] Feldman, E. E., Hornbeck, R. W., and Osterle, J. F., "A Numerical Solution of Developing Temperature for Laminar Developing Flow in Eccentric Annular Ducts," *International Journal of Heat and Mass Transfer*, Vol. 25, No. 2, 1982, pp. 243-253.

[14] Synder, W. T. and Goldstein, G. A., "An Analysis of Fully Developed Laminar Flow in an Eccentric Annulus," *A.I.Ch.E. Journal*, Vol. 11, 1965, pp. 462-467.

[15] Prusa, J. and Yao, L. S., "Natural Convection Heat Transfer Between Eccentric Horizontal Cylinders," ASME Paper 82-HT-43, St. Louis, Mo., June 1982.

[16] Synder, W. T., "An Analysis of Slug Flow Heat Transfer in an Eccentric Annulus," *A.I.Ch.E. Journal*, Vol. 9, 1963, pp. 503-506.

[17] El-Saden, M. R., "Heat Conduction in an Eccentrically Hollow, Infinitely Long Cylinder with Internal Heat Generation," *Journal of Heat Transfer*, Vol. 83, 1961, pp. 510-512.

[18] Redberger, P. J. and Charles, M. E., "Axial Laminar Flow in a Circular Pipe Containing a Fixed Eccentric Core," *Canadian Journal of Chemical Engineering*, Vol. 40, 1962, pp. 148-151.

[19] Jackson, R. H. and Synder, W. T., "Laminar Heat Transfer in an Eccentric Annulus with Constant Heat Flux Boundary Condition," *Proceedings of the Tenth Southeastern Conference on Theoretical and Applied Mechanics*, Vol. 10, 1980, pp. 557-579.

[20] Pepper, D. W. and Cooper, R. E., "Numerical Solution of Recirculating Flow by a Simple Finite Element Recursion Relation," *Computers and Fluids*, Vol. 8, 1980, pp. 213-223.

[21] Gazdag, J., "Numerical Convective Schemes Based on Accurate Computation of Space Derivatives," *Journal of Computational Physics*, Vol. 13, 1973, pp. 100-113.

[22] Myers, R. B., Taylor, T. D., and Murdock, J. W., "Pseudospectral Simulation of a Two-Dimensional Vortex Flow in a Stratified, Incompressible Fluid," *Journal of Computational Physics*, Vol. 43, 1981, pp. 180-188.

[23] Swartztrauber, P. and Sweet, R., "Efficient FORTRAN Subprograms for the Solution of Elliptic Partial Differential Equations," NCAR Tech. Note, TN/IA-109, 1975.

[24] Cooley, J. W. and Tukey, J. W., "An Algorithm for the Machine Calculation of Complex Fourier Series," *Mathematics of Computation*, Vol. 19, 1965, pp. 297-301.

[25] Kuehn, N. H. and Goldstein, R. J., "An Experimental Study of Natural Convection Heat Transfer in Concentric and Eccentric Horizontal Cylindrical Annuli," *Journal of Heat Transfer*, Vol. 100, 1978, pp. 635-640.

[26] Kuehn, T. H. and Goldstein, R. J., "An Experimental and Theoretical Study of Natural Convection in the Annulus between Horizontal Concentric Cylinders," *Journal of Fluid Mechanics*, Vol. 74, 1976, pp. 695-719.